



The computation of reference state and APE production by diabatic processes in an idealised tropical cyclone

K. C. Wong*, Rémi Tailleux, Suzanne L. Gray

Correspondence to: K C Wong, Department of Meteorology, University of Reading, RG6 6BB, UK. E-mail: k.c.wong@pgr.reading.ac.uk

This study investigates the energetics of tropical cyclone intensification using the Available Potential Energy (APE) theory. While the idea that tropical cyclones (TCs) intensify as the result of the conversion into kinetic energy of the available potential energy (APE) generated by the release of latent heat extracted from the warm tropical ocean surface is now well accepted, its rigorous theoretical formalisation has remained elusive owing to the complexity of constructing a suitable reference state for defining and quantifying APE in a moist atmosphere. Yet, the construction of such a reference state is a key fundamental issue, because the magnitude of the APE reservoir and of its temporal evolution, as well as the values of the thermodynamic efficiencies controlling the rate at which diabatic processes generate or destroy APE, depend on its specification. This issue is illustrated in the idealised context of an axisymmetric TC model by comparing the energetics of TC intensification obtained by using two different sorting-based approaches to compute the reference state defining APE. It is found that the thermodynamic efficiency controlling the APE generation by surface latent heat fluxes is larger when the reference state is constructed using a ‘top-down’ sorting method, as the APE thus defined absorbs all the CAPE present in the system. However, because a large fraction of the overall CAPE is never released during the TC’s lifetime (e.g. in regions dominated by subsidence), there is a better agreement between the production of APE by surface fluxes and its subsequent conversion into kinetic energy when a ‘bottom-up’ reference state is used. These results suggest that contrary to what is usually assumed, the reference state in APE theory should be constructed to *minimise*, rather than maximise, the total APE, so that the introduction of dynamically inert APE is minimised.

Key Words: Tropical cyclone; Available potential energy; Reference state; CAPE; Intensification

Received ...

1. Introduction

A mature tropical cyclone (TC) is often characterised by a well developed secondary circulation. At the surface, air flows cyclonically towards the vortex core. The surface convergence is balanced by rising motion in deep convection within the eyewall, followed by anti-cyclonic outflow in the upper troposphere and subsidence in regions at larger radii. As surface air spirals inward, sensible and latent heat are extracted from the ocean surface through surface fluxes. The latent heat is later released as the air rises within the eyewall which strengthens the convective updraughts, leading to stronger surface inflow and eventually maintains a thermally direct secondary circulation (see Emanuel (1991) or Emanuel (2003) for detailed review).

Emanuel (1986) first suggested that the secondary circulation of a TC vortex can be viewed as a four strokes Carnot engine that converts energy acquired from the ocean into mechanical energy. In brief, as an surface air parcel moves down the pressure gradient

towards the vortex core it extracts energy from the ocean surface and expands isothermally. Upon reaching the base of the eyewall, the air parcel rises within the deep convection where it expands and cools adiabatically. The air parcel then enters the outflow channel near the tropopause. As it moves away from the vortex core, it compresses isothermally and loses energy to space by radiative cooling. The circulation is finally completed by sinking back to the surface at large radius where the parcel is warmed by adiabatic compression. In this view, the maximum amount of work that can be performed is given by the Carnot efficiency defined as $(T_s - T_{out})/T_s$, where T_s represents the parcel’s temperature in the surface inflow and T_{out} is its temperature in the upper-tropospheric outflow (see Ozawa and Shimokawa (2015) for a recent extension of this idea).

From an energetic viewpoint, the Carnot approach can be used to simplify the vortex’s energy budget into a two terms balance between energy production and mechanical dissipation. For example, Emanuel (1988) proposed the ‘Maximum Potential

Intensity' (MPI) theory that aims to predict the maximum possible intensity of a TC in a given atmospheric state. The MPI theory assumes the surface energy input is converted into mechanical energy at the Carnot efficiency, which is in theory the highest efficiency possible. Therefore, by equating such energy conversion to the mechanical dissipation one can predict the maximum possible intensity of the vortex. See Smith *et al.* (2008) for a critical review of the MPI theory.

Another interesting characteristic of Emanuel's Carnot approach is the realisation that surface energy fluxes can be linked to their conversion into mechanical energy by the thermodynamic efficiency. The thermodynamic efficiency in Emanuel's Carnot approach is determined by the temperature of the surface inflow and that in the upper-tropospheric outflow (i.e. T_s and T_{out}). In Emanuel's original framework, air parcels are assumed to circulate in a fixed path such that T_s and T_{out} are assumed to be constant. Generally, T_s is mostly controlled by the sea surface temperature while locally it can be affected by localised processes such as precipitation downdraughts. Meanwhile, T_{out} is mostly determined by how high an air parcel can rise in the eyewall convection, or simply the buoyancy of an air parcel. However, in a more realistic setting when air parcels do not follow the same trajectory in the secondary circulation, the thermodynamic efficiency is likely to vary across the vortex depending on the buoyancy of individual air parcel.

As is well known from classical thermodynamic theory, the Carnot theory of heat engines arises from the consideration of the entropy budget applied to a system undergoing a closed thermodynamic cycle. As a result, a TC can be regarded as a Carnot heat engine only when viewed over its entire life cycle for the assumption of a closed cycle to be approximately satisfied. The approach is therefore difficult to apply to the study of the transient evolution and intensification of TCs. The theory of Available Potential Energy (APE), first introduced by Lorenz (1955) for understanding how the large-scale atmospheric circulation is maintained against dissipation, represents in principle a more satisfactory approach to study the energetics of stratified fluids, e.g., Tailleux (2013a) *. Physically, this is because APE is by definition the fraction of the total potential energy convertible into kinetic energy, and hence ultimately responsible for the observed intensification. Historically, APE has been primarily defined as the difference between the potential energy of the actual state minus that of a notional reference state obtained by means of a (moist) adiabatic re-arrangement of the fluid parcels minimising the total potential energy of the system. In the case of a dry and statically stable atmosphere, Lorenz (1955) demonstrated that the APE resides only in the horizontal gradient of temperature and pressure such that the reference state can be represented by the horizontal average of pressure and temperature fields.

For a moist atmosphere, Lorenz (1978, 1979) and Randall and Wang (1992) have argued that the presence of boundary layer parcels with Convective Available Potential Energy (CAPE) complicates the definition of APE, as it makes it possible for the atmosphere to possess APE even for a horizontally homogeneous barotropic state. This implies, therefore, that CAPE induces a vertical component to APE. The connection between the two concepts was discussed in much details in Emanuel (1994). However, since it is not generally possible for all the CAPE that exists at any given time in the atmosphere to be released, it seems obvious that absorbing all the CAPE into the definition of moist APE, as proposed by Lorenz (1978, 1979) and Randall and Wang (1992) may result in a value of APE possibly

greatly overestimating the amount of potential energy that can be converted into kinetic energy. Physically, the APE theory would have a greater predictive value if APE could be defined to represent the 'right' fraction of the total potential energy actually convertible into kinetic energy, which is the basic idea explored in this paper.

Lorenz (1978) suggested that one way to construct the reference state for a moist atmosphere is to use a 'sorting' procedure that rearranges all air parcels in the atmosphere adiabatically into a hydrostatic and statically stable column. Various studies such as Randall and Wang (1992) and Tailleux and Grandpeix (2004) used similar adiabatic rearrangement to compute the reference state and APE of a conditionally unstable atmospheric column but it is unclear how such techniques can be applied to a realistic three-dimensional atmosphere. Also, note that the APE theory and the concept of reference state here are defined globally over the entire volume of the atmosphere. Meanwhile, CAPE is usually defined locally for a given air parcel by lifting it along a moist adiabat under the action of a positive buoyancy anomaly with respect to the local sounding without altering the surrounding atmosphere. Therefore, although APE may include contribution from CAPE in a moist atmosphere, they are two completely different concepts. Recently, the possibility of using a more general reference state in conjunction with a locally-defined 'APE density' has been discussed in Tailleux (2013a,b) and Peng *et al.* (2015) but the APE density will not be covered in this study.

As far as we are aware, Pauluis (2007) is the only study that fully generalises the discussion of sinks and sources of APE for a general moist atmosphere, but it provides no details about how to construct the reference state on which the theory relies. Assuming that a suitable reference state can be constructed, the discussion of energetics in APE theory takes the form

$$\frac{d APE}{dt} = G - C_{APE \rightarrow KE}, \quad (1)$$

$$\frac{d KE}{dt} = C_{APE \rightarrow KE} - D \quad (2)$$

where d/dt is the total time derivative, APE and KE represent volume integrated values of APE and kinetic energy, and D denotes dissipation by viscous processes. Equation (1) shows that the change in APE in the atmosphere ($dAPE/dt$) is controlled by the balance between the production of APE by diabatic processes such as surface fluxes (G) and the conversion of APE into kinetic energy ($C_{APE \rightarrow KE}$). Pauluis (2007) also presented a detailed investigation of the production of APE by diabatic processes in a moist atmosphere. In general, the production of APE is governed by the addition (or removal) of heat and moisture by diabatic processes multiplied by a thermodynamic efficiency defined as $(T_1 - T_{ref})/T_1$. This is very similar to Emanuel's Carnot efficiency with T_s and T_{out} replaced by the in-situ temperature of an air parcel (T_1) and its temperature in the reference state after the adiabatic rearrangement (T_{ref}). Note that for a dense air parcel that is rearranged downward in the reference state, T_{ref} can be warmer than T_1 resulting a negative thermodynamic efficiency. Another key difference is that each air parcel in the atmosphere will have a different position in the reference state leading to a range of thermodynamic efficiencies depending on their buoyancy. For the sake of clarity, the thermodynamic efficiency $(T_1 - T_{ref})/T_1$ will be referred to as the 'APE production efficiency' in this study. Kinetic energy (KE), on the other hand, grows as a result of the conversion of APE into kinetic energy, and decays as the result of viscous dissipation D , usually assumed to be primarily controlled by surface drag.

Based on the APE theory, this paper aims to investigate the production of APE by diabatic processes and its conversion into

* Interestingly, Ozawa *et al.* (2003) suggest that the second law and Lorenz APE theory are nearly equivalent, but the consideration of the ocean budget, e.g., Tailleux (2010), clearly shows that this is not true in general, and hence that one should be cautious in assuming that the two are interchangeable.

kinetic energy in numerical simulation of an idealised TC vortex. The complexity associated with finding a suitable reference state of a moist atmosphere with the adiabatic rearrangement approach is also addressed. The choice of the reference state is important, because it affects the values of the APE reservoir, as well as of the generation term G in (1). **On the contrary, the conversion of APE into kinetic energy ($C_{APE \rightarrow KE}$) is independent from the choice of reference state.** To understand why it matters, let us integrate (1) and (2) over the life cycle of the TC, assuming the kinetic energy to be small at the beginning and end of the life cycle, which yields

$$\Delta APE = \overline{G} - \overline{C}_{APE \rightarrow KE} \quad (3)$$

$$0 \approx \overline{C}_{APE \rightarrow KE} - \overline{D}, \quad (4)$$

where ΔAPE represents the net change of APE over the life cycle of the TC and \overline{G} , $\overline{C}_{APE \rightarrow KE}$ and \overline{D} are the production, conversion and dissipation terms integrated over the volume and time. Combining these two equations yields

$$\overline{G} \approx \overline{D} + \Delta APE \quad (5)$$

This formula is similar to that underlying MPI theory, but for the presence of the net APE change term ΔAPE . Physically, one would expect ΔAPE to be negligible in order to be able to directly link generation and dissipation, but this is not necessarily the case depending on how the reference state is constructed. For instance, the initial and end states could both possess significant amounts of CAPE that is not released due to the presence of convective inhibition. Absorbing such inert CAPE in the definition of APE could give the illusion of a physically meaningless large value of ΔAPE .

The main question investigated in this paper is whether it is possible to construct the reference state such as to minimise ΔAPE , which would establish the possibility of using APE theory to provide an alternative rigorous theoretical construction of MPI theory. Two different sorting methods with contrasting views on buoyancy are developed and used to analyse the output from an idealised TC numerical model. The production of APE by surface fluxes in the simulated TC is also investigated using the Pauluis (2007) APE framework. The production of APE by surface sensible and latent heat fluxes is computed and compared to the conversion into kinetic energy.

This paper is divided into the following sections. Section 2 gives a brief introduction to the numerical TC model and the sorting methods. Section 3 shows the main results of the investigation followed by a conclusion and discussion in section 4.

2. Methodology

2.1. Axisymmetric tropical cyclone model

This study used a modified version of the axisymmetric TC model (hereafter 2D model) designed by Rotunno and Emanuel (1987). Modifications to the rain-physics scheme and gravity wave filter following Craig (1996) and Craig and Gray (1996) were also included. The simulation follows the typical ‘prototype problem’ setup. The atmosphere was initialised using the mean hurricane season sounding (Jordan 1958) and a weak initial vortex with maximum surface wind speed no stronger than 15 ms^{-1} was placed over an open ocean surface. The sea surface temperature was fixed at 29°C throughout the simulation.

The 2D model contains nine prognostic variables including velocities in the radial, azimuthal and vertical directions (u , v , w),

potential temperature (θ), a dimensionless Exner pressure deviation from initial state (π), and the mixing ratios of water vapour (r_v), cloud water (r_l), rain water (r_r) and ice (r_i). The prognostic equations were integrated forward in time with a time step of 6 seconds for a simulation duration of 150 hours. A shorter time step (0.6 seconds) was used for advancing w , u and π to account for acoustic waves. No parametrisation scheme was used for convection as it is simulated explicitly. The 2D model domain extends radially to 3600 km and vertically to 27.5 km with a horizontal grid spacing of 2.5 km and vertical grid spacing of 0.625 km. Note that each grid box in the axisymmetric domain represents a ring shaped volume around the centre of rotation. A no-flux boundary condition was used while ‘sponge layers’ were placed at the top and outer boundaries for the absorption of gravity waves. Surface fluxes were simulated using the bulk aerodynamic formulae. For sensible and latent heat flux, the flux coefficients were set at 0.001 and 0.0012. **For surface friction, the drag coefficient (C_D) was computed using**

$$C_D = 1.1 \times 10^{-3} + 4 \times 10^{-5} \times (u^2 + v^2)^{1/2} \quad (6)$$

in which u and v are evaluated at the lowest model level.

2.2. Behaviour of the simulated vortex

The evolution of maximum surface wind speed and minimum surface pressure of the simulated vortex can be divided into three distinct stages (figure 1a). The first 40 hours was a stagnation stage with little to no intensification. This was followed by a rapid intensification stage between 40-60 hours. The maximum surface wind speed increased from just above 20 ms^{-1} at 40 hours to nearly 70 ms^{-1} at 60 hours while the minimum surface pressure reduced rapidly from 980 mb to 940 mb towards the end of the rapid intensification. After the rapid intensification, the vortex was in a near steady state from 60 hours onwards with small fluctuations in intensity. It reached a maximum intensity of 83 ms^{-1} at 84 hours and remained above 60 ms^{-1} for the rest of the simulation.

Figure 1b shows the radius-height cross-section of horizontal wind speed at 120 hours. The eye of the mature vortex is a calm region with wind speed below 10 ms^{-1} . Surrounding the eye is the eyewall, represented by a narrow region of strong wind reaching up to 70 ms^{-1} and confined within 50 km from the centre of rotation. In general, the rate of intensification and structure of the simulated vortex is similar to other numerical simulations of the prototype problem using 2D (e.g. Bryan and Rotunno (2009)) and 3D (e.g. Nguyen *et al.* (2008); Shin and Smith (2008)) TC models.

Figure 2a-b shows the radius-time plot of u and equivalent potential temperature θ_e of the lowest model level. From 40 hours onwards, the surface layer within 500 km radius is characterised by negative values of u , representing the surface inflow branch of the secondary circulation. However, multiple outflows were also observed in the surface layer at 20-30 hours (200-900 km radius), 60-80 hours (200-2000 km radius) and 100-120 hours (1500-2000 km radius) respectively. These surface outflows were marked by positive values of u reaching $3\text{-}5 \text{ ms}^{-1}$. They tend to form at about 250 km radius and then propagate away from the centre of the vortex at a fairly constant speed of 25-35 km per hour.

Comparing figure 2a and 2b show that the surface outflows clearly affected the values of θ_e in the surface layer. While the highest values of θ_e ($> 365 \text{ K}$ in the mature vortex) can be found near the centre of rotation, the region beyond 500 km radius is dominated by continuous fluctuation between higher ($> 355 \text{ K}$) and lower ($< 350 \text{ K}$) values of θ_e throughout the simulation. The fluctuation is characterised by a gradual increase in θ_e values to a

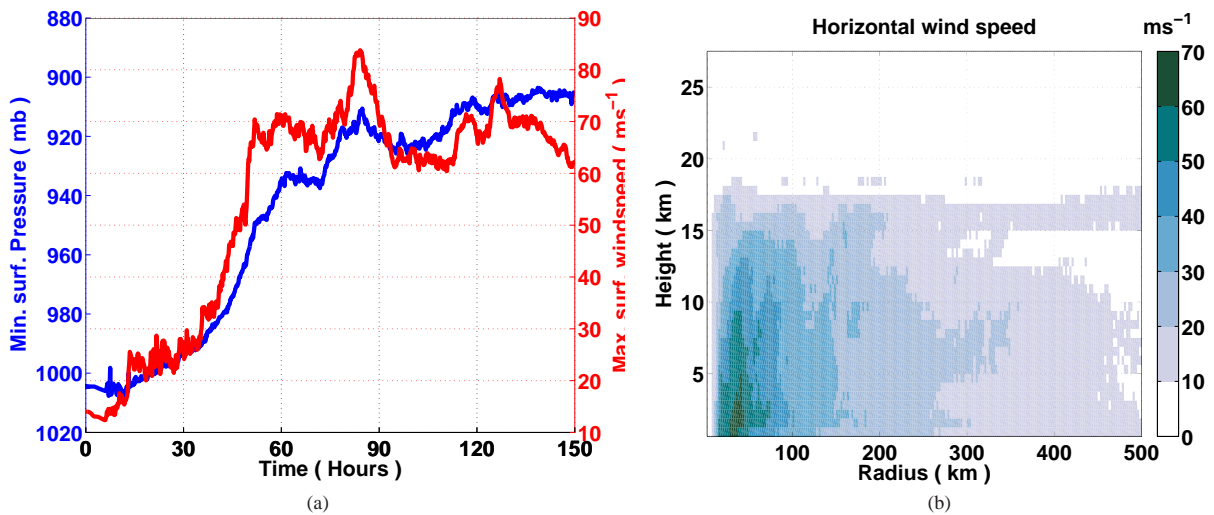


Figure 1. Simulation results: a) Time series of minimum surface pressure (blue) and maximum surface wind speed (red); b) Distribution of horizontal wind speed in the vortex after 120 hours of simulation.

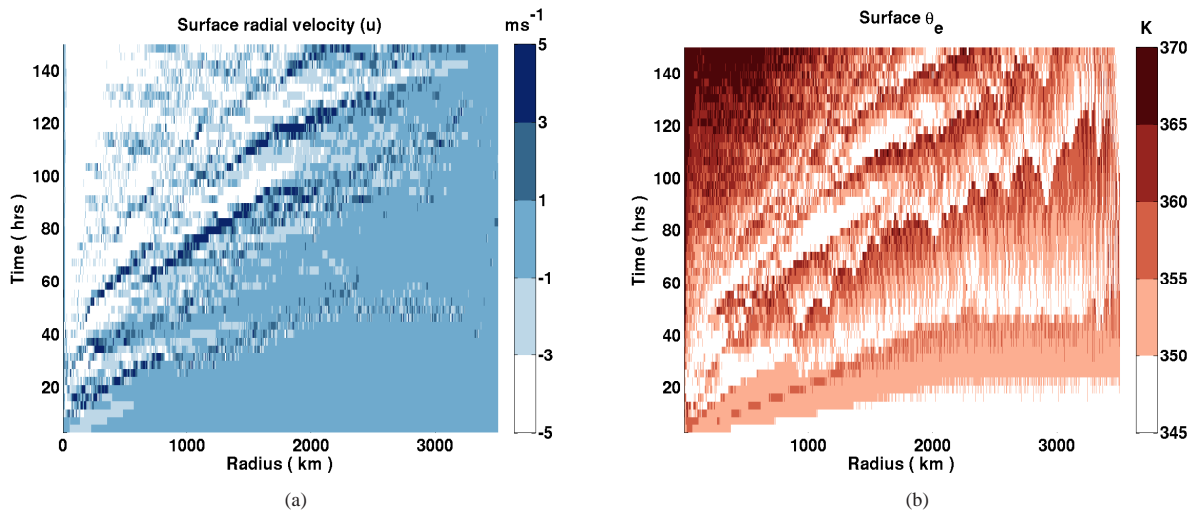


Figure 2. Radius-time plot of a) radial velocity (u) and equivalent potential temperature (θ_e) in the lowest model level.

maximum of roughly 360 K. The time of maximum θ_e is usually observed during the onset of surface outflow. An abrupt drop in θ_e to below 350 K is then observed after each surface outflow, followed by a gradual recharge until the next surface outflow. The clear outward propagation signal suggests that the variations in u and θ_e might be associated with a gravity wave signal originating from the inner region of the vortex, although more work would be required to confirm that such a propagation can indeed be interpreted in terms of a ‘physical’ wave and is not a numerical artifact.

2.3. Sorting strategies for computing Lorenz reference state

The definition of the reference state and how it can be derived from the observed atmospheric state is a vital part of the APE theory. As discussed in Lorenz (1955, 1978), one possible approach is the ‘sorting’ method in which air parcels in the atmosphere are rearranged adiabatically according to their buoyancy. Eventually, this will produce a hydrostatic and statically-stable column of air such that no more total potential energy can be used to support circulation thus satisfying the definition of the reference state. As recently considered in the oceanic case by Saenz *et al.* (2015), there are two natural sorting strategies, namely the ‘top-down’ and ‘bottom-up’ sorting methods.

Consider a two-dimensional atmosphere containing four air parcels (figure 3a). To construct the reference state, the top-down

sorting method begins by lifting all four air parcels adiabatically and reversibly to the top of the atmosphere represented by pressure $P_{ref,top}$ (figure 3b). The most buoyant air parcel (parcel 1) after the relocation is assigned to the pressure level $P_{ref,top}$ and removed from the pool of parcels. The same process is then repeated with parcels 2–4 at the next pressure level $P_{ref,top} + \delta P$ and then continuing downward (figure 3c). Eventually each air parcel is assigned to a pressure level, resulting in a sorted air column that represents the reference state (figure 3d). However, one could argue that the reversal of the top-down sorting method can also produce a valid reference state. In this case, the bottom-up sorting method constructs the reference state by bringing all four parcels downward to the surface represented by $P_{ref,bot}$. The least buoyant air parcel (parcel 4) is assigned to this pressure level and removed from the pool. The process is then repeated with parcels 1–3 at the next pressure level $P_{ref,bot} + \delta P$ and continuing upward until the construction is finished. Note that although both sorting methods give the same result in figure 3d, this is not always the case in practice due to the presence of CAPE and each sorting method will produce a different reference state. This is the major focus of this paper and will be demonstrated further in the next section.

Although the two sorting methods appear to be the polar opposite of each other, their operating principles are identical. In brief, grid boxes of the 2D model at a given integration time are regarded as individual air parcels. For both sorting methods,

the values of in-situ air temperature (T_1), pressure (P_1) and total mixing ratio r_{tot} are used to compute the liquid potential temperature $\theta_l(T_1, P_1, r_{tot})$ of all air parcels in the model domain. The air parcels are then relocated adiabatically and reversibly to the starting P_{ref} (e.g. $P_{ref,bot}$ or $P_{ref,top}$) by conserving $\theta_l(T_1, P_1, r_{tot})$, r_{tot} and mass. The choice of using θ_l as a conserved variable in the adiabatic relocation is because θ_l is defined as an exact proxy for moist entropy (η) such that it satisfies $\eta(\theta_l, P_0, r_{tot}) = \eta(T_1, P_1, r_{tot})$ where P_0 is the surface pressure. This coincides with the definition presented in Emanuel (1994) if the air parcel brought adiabatically to P_0 is unsaturated.

The parcel's temperature after the relocation, T_{ref} , as well as the partition between vapour and liquid mixing ratio, r_v and r_l , are then computed. An iteration procedure is designed using the fact that θ_l and r_{tot} are conserved in the relocation (i.e. $\theta_l(T_1, P_1, r_{tot}) = \theta_l(T_{ref}, P_{ref}, r_{tot})$) such that T_{ref} and the new vapour-liquid partition can be computed iteratively from a range of possible values. The densities of the air parcels after the relocation $\rho(P_{ref}, T_{ref}, r_{tot})$ are then computed and the densest (or lightest for the top-down sorting method) parcel is selected and assigned to the current P_{ref} level. The next P_{ref} level is then computed using $P_{ref} - \delta P$ (or $P_{ref} + \delta P$ for the top-down sorting method) where δP is the difference in pressure between the current and the next P_{ref} level calculated using the mass of the selected parcel and the hydrostatic relationship. After removing the selected air parcel from the pool, the remaining parcels are relocated to the updated P_{ref} thus starting the next relocation cycle. This process is repeated until all air parcels are assigned to a P_{ref} slot, resulting a hydrostatic and statically stable column of air parcel representing the reference state.

The pressure at the bottom and top of the reference state, $P_{ref,bot}$ and $P_{ref,top}$, can be expressed as $P_{ref,top} = P_{ref,bot} - \Delta P$. $P_{ref,bot}$ can be computed using the relationship between surface pressure and the total mass of air over a given surface area while ΔP can be computed using the total mass of atmosphere in the model domain and the hydrostatic relationship. Both terms can be expressed as

$$P_{ref,bot} = \frac{\sum(P_i \times A_i)}{A_{tot}}, \quad (7)$$

$$\Delta P = \frac{\sum(m_i \times g)}{A_{tot}},$$

where P_i , A_i and m_i are the surface pressure, surface area and mass of the i^{th} column of the 2D model domain, g is gravity and A_{tot} is the total surface area of the model domain. Note that both $P_{ref,bot}$ and $P_{ref,top}$ (and any other P_{ref} levels in the sorted column) are horizontally homogeneous such that no more horizontal pressure gradient force (PGF) can further contribute to the APE in the atmosphere.

Both the top-down and bottom-up sorting methods were used to analyse the output from the 2D model. To improve computational efficiency, only the lower portion of the model domain was analysed while a large number of grid boxes representing the stratosphere were ignored. The cutoff height was set at 15 km above sea level such that the analysis includes most, if not all, of the troposphere and the important features of the simulated vortex.

3. Results

3.1. Reference states

Figure 4 shows the reference state position of each air parcel produced using both sorting methods at 60 and 120 hours into the simulation. The reference state position of an air parcel is represented by the pressure slot P_{ref} it occupies in the sorted column. For both sorting methods, a small P_{ref} value indicates an air parcel is relatively buoyant compared to the rest of the domain and is lifted upward in the reference state. Similarly, a large P_{ref} value suggests an air parcel is relatively dense and is relocated towards the surface in the reference state.

Using the top-down sorting method, buoyant air parcels with small P_{ref} values can be found near the surface at 60 hours when the vortex has just finished its rapid intensification (figure 4a). The surface parcels were able to reach a small P_{ref} because the CAPE stored in the boundary layer was released when the surface parcels were lifted upward during the top-down sorting. Also, parcels between 6-10 km above sea level near the centre of rotation were mostly lifted to smaller P_{ref} compared to those at larger radii, indicating this part of the vortex was relatively buoyant compared to the region further away from the centre of rotation. While surface parcels rely on the release of CAPE during the adiabatic rearrangement to reach a small P_{ref} , parcels near the centre of rotation are in general thermally buoyant due to the warm core signature of the vortex and therefore lifted upward in the reference state.

At 120 hours, the vortex has further developed and reached a near steady state intensity. At this time, the surface layer is still very buoyant with most parcels lifted to small P_{ref} especially in the inner region within 1000 km radius. However, the number of parcels with small P_{ref} values has reduced slightly in the region between 1000 and 2000 km radius (figure 4b). This could be related to a surface outflow event which reduced the θ_e of the region at 120 hours (see figure 2b).

At 8-14 km above sea level, the inner region of the vortex remained relatively buoyant compared to the rest of the model domain with the number of air parcels showing small P_{ref} values increased slightly as the vortex intensified. Another notable difference compared to the earlier time is the presence of model columns within 1000 km radius which have smaller P_{ref} values than the surrounding environment. These buoyant air columns

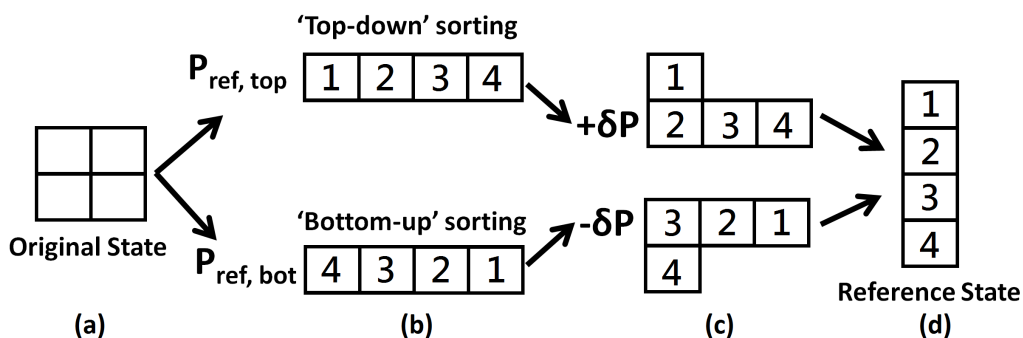


Figure 3. Graphical illustration of the top-down and bottom-up sorting method. See text for explanation.

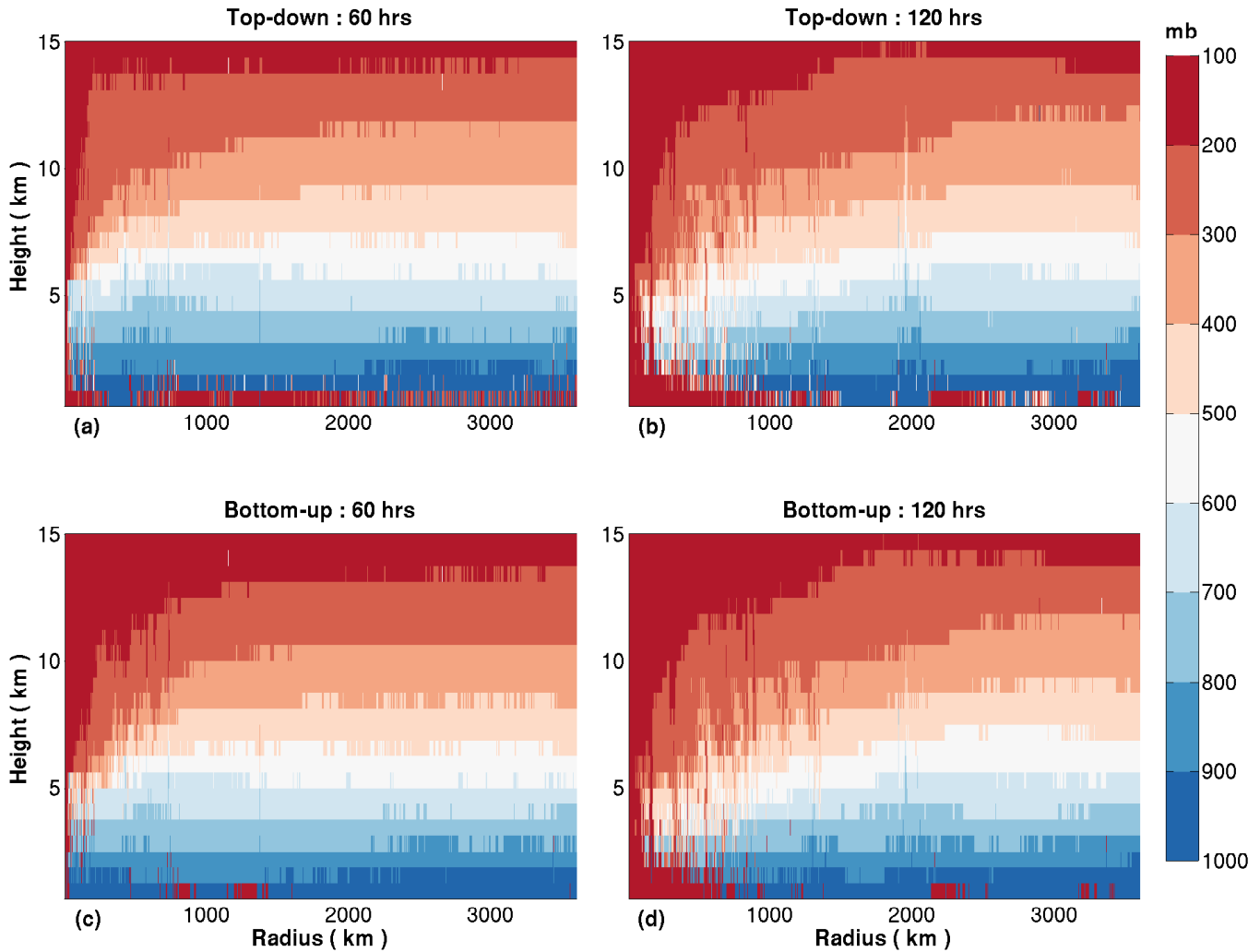


Figure 4. Reference state position represented by P_{ref} computed using the top-down (a-b) and bottom-up (c-d) sorting methods at 60 and 120 hours respectively.

are rings of weaker convection outside the eyewall in which the release of latent heat increases the buoyancy of air parcels, resulting in a smaller P_{ref} in those model columns.

Similarly, the value of P_{ref} was computed using the bottom-up sorting method at both 60 and 120 hours (figure 4c-d). Above the boundary layer, the results at both integration times are generally similar to those produced by the top-down sorting method. The mid to upper-atmosphere (beyond 5 km above sea level) within 1000 km radius is characterised by an anvil shaped region of buoyant air parcels with P_{ref} values smaller than 200 mb. Also, model columns with smaller P_{ref} values can be found within 1000 km radius just outside the eyewall at 120 hours which is similar to the top-down result described previously. However, the most remarkable difference to the results with the top-down sorting method is the lack of buoyant parcels with small P_{ref} values near the surface when using the bottom-up sorting method. At 60 hours, only two localised patches of parcels with small P_{ref} values are found in the surface layer at 800 and 1200 km radius. At 120 hours, the number of surface parcels with small P_{ref} values increased in the inner region but the surface layer further away from the centre of rotation is still dominated by parcels with larger P_{ref} values compared to the top-down results.

To further investigate the different distributions of air parcels in the reference states computed by both sorting methods, the model domain was divided into three regions representing the surface layer (i.e. lowest model level), the inner region (radius ≤ 1000 km) and the outer region (radius > 1000 km). Figure 5 shows a scatter plot of P_{ref} against the in-situ pressure (P_1) for both sorting methods at 120 hours. Each grid box is coloured according to its origin using the division above.

In general, the distribution of air parcels in the reference states computed by both sorting methods are very similar. Buoyant air parcels in the inner region (dark grey) were lifted upward to P_{ref} slots that are smaller than their in-situ pressure while air parcels in the outer region (light grey) showed only small displacement as they are relatively stable. Similar to the difference in the values of surface P_{ref} , the most remarkable difference between both sorting methods is the distribution of surface parcels (black) in the reference state. A large number of surface parcels were lifted to the top of the reference state between 300 and 100 mb when using the top-down sorting method while most of them remained near the surface when using the bottom-up sorting method. Another notable difference is that when using the top-down sorting method, some parcels from the surface and the inner region were relocated to the middle of the reference state between 600 and 400 mb which was not observed when using the bottom-up sorting method.

As the buoyancy of the surface air parcels is largely determined by the amount of CAPE they possess, the different results produced by the two sorting methods are clearly related to the treatment of CAPE during the adiabatic relocation. In the top-down sorting method, the starting pressure $P_{ref,top}$ is usually around 30 mb which is way above the typical lifting condensation levels (LCLs) of the surface parcels. Therefore, when the surface parcels were brought adiabatically upward to the upper troposphere, they were able to release most if not all the latent heat they have. This has a huge impact on the density of an surface air parcel after the adiabatic relocation since the potential contribution from surface CAPE is included. Therefore, the top-down sorting method offers a maximising view on the buoyancy

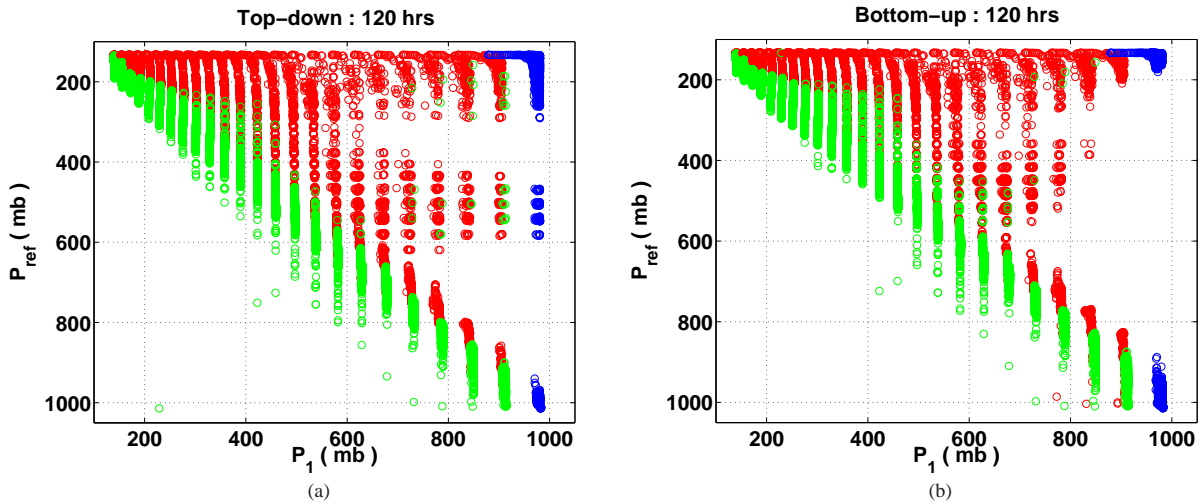


Figure 5. Scatter plot of P_{ref} against in-situ pressure P_1 for a) the top-down sorting method and b) the bottom-up sorting method at 120 hours. Each symbol represents a model grid box and the model domain was divided into the following regions: surface layer (blue); above surface layer and within 1000 km radius (red); above surface layer and beyond 1000 km radius (green).

of surface air parcels by assuming all CAPE in the surface layer can be released in the sorting process.

In contrast, when air parcels were brought to the surface in the bottom-up sorting method, they were warmed by the adiabatic compression. As a result, air parcels were mostly unsaturated after the relocation thus unable to release latent heat. Therefore, only the most buoyant surface parcels were able to reach their LCL after the P_{ref} slots below the LCL were filled by denser surface parcels from the outer region beyond 1000 km radius. As a consequence, the bottom-up sorting method generally excludes the potential contribution from CAPE when evaluating the buoyancy of surface air parcels, leading to the lack of surface parcels with small P_{ref} values. Compared to the top-down sorting method, the bottom-up sorting method offers a more minimising view on the buoyancy of surface air parcels by placing a much harder restriction on the release of CAPE. Since both sorting methods were able to identify the buoyant parcels in the upper part of the inner region, it is clear that the construction of reference state based on a parcel sorting approach is not affected by the thermal buoyancy that is directly available but the treatment of potential buoyancy associated with CAPE is more challenging. The results here highlight the complexity of finding the reference state of a moist atmosphere due to the presence of CAPE. In the next section it will be showed that the contrasting view on buoyancy from the sorting methods has a large impact on the computation of APE production by surface fluxes.

3.2. APE production efficiency

After constructing the reference state, the APE production efficiency, defined as $(T_1 - T_{ref})/T_1$, is computed for both sorting methods. In general, the APE production efficiency reflects the buoyancy of an air parcel compared to the rest of the atmosphere since the difference between T_1 and T_{ref} is determined by how the parcel is rearranged in the reference state. A buoyant air parcel that is relocated upward in the reference state will have a cooler T_{ref} compared to the in-situ temperature T_1 leading to a positive APE production efficiency. In contrast, a dense air parcel that is relocated towards the surface will have a warmer T_{ref} thus a negative APE production efficiency.

Consistent with the distribution of parcels with small P_{ref} values, air parcels with the highest APE production efficiency were found in the surface layer and in the mid to upper-troposphere inside the inner region when using the top-down sorting method at both 60 and 120 hours (figure 6a-b). The

APE production efficiency of individual surface parcels can be as high as 0.3, while most of the buoyant parcels in the mid to upper troposphere of the inner region showed values between 0.1-0.2. Beyond 500 km radius, the mid to upper-troposphere is characterised by a weak negative APE efficiency. This is because the relatively stable air parcels in the outer region were relocated downward to make room for the buoyant air parcels from the surface and the inner region that were relocated to the top of the reference state. The compression and warming caused by the downward relocation resulted a larger T_{ref} compared to the in-situ temperature T_1 , thus a negative APE efficiency.

As the bottom-up sorting method restricts the release of surface CAPE during the sorting process, most of the surface parcels remained near the surface in the reference state (figure 6c-d). **In the surface layer, the values of APE production efficiency are generally much less than those computed with the top-down sorting method with most parcels showing values between ± 0.15 at both integration times.** Meanwhile, positive APE production efficiency was found between 6-12 km above sea level in the inner region for both integration times. Compared to the top-down results, the bottom-up sorting method clearly produced more parcels with positive APE production efficiency in the mid to upper troposphere. This is particularly obvious at 120 hours as the anvil of parcels with positive APE production efficiency extended further outward compared to the top-down results at the same integration time. This suggests the restriction on surface CAPE release during sorting will not only affect the reference state position of surface parcels but also those in the mid to upper troposphere.

Figure 7a shows the time series of the area-averaged APE production efficiency over the surface layer for both sorting methods. In general, the top-down sorting method produced a much higher average surface APE production efficiency since more surface parcels were relocated upward and attained a smaller T_{ref} by releasing CAPE. After an initial spike up to 0.22 in the first 20 hours, the average surface APE production efficiency reduced slowly to 0.15 at the end of the simulation. **There were also signs of periodic fluctuation with a period of roughly 20-40 hours.**

Figure 7b shows the time series of the area-averaged top-down surface APE production efficiency over the inner and outer region respectively. **When averaging over the inner region only, the surface APE production efficiency increased steadily from 30 hours onwards due to the build up of CAPE by the continuous surface moisture flux. In contrast, the time series produced using**

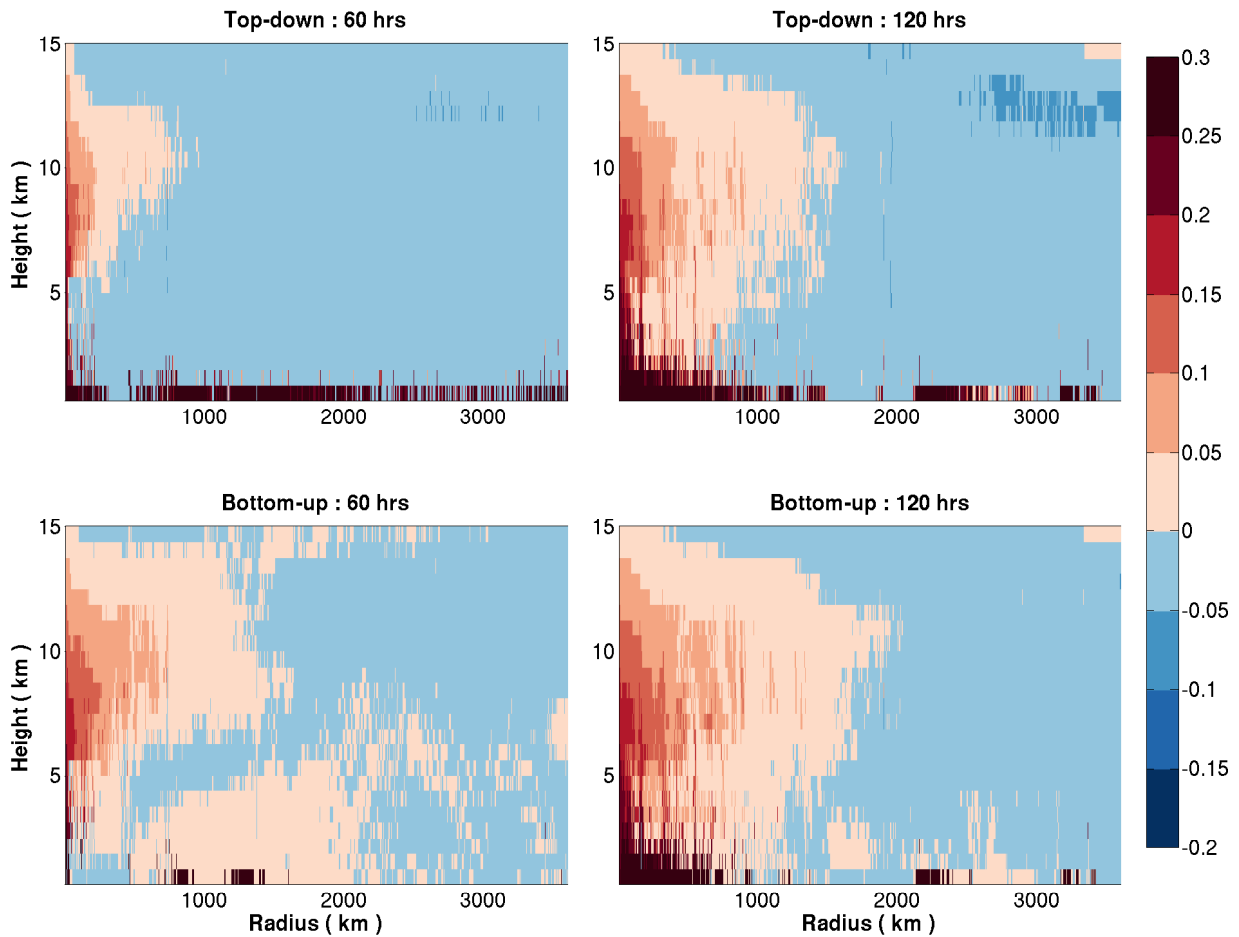


Figure 6. APE production efficiency $(T_1 - T_{ref}) / T_1$ computed using the top-down (a-b) and bottom-up (c-d) sorting method at 60 and 120 hours.

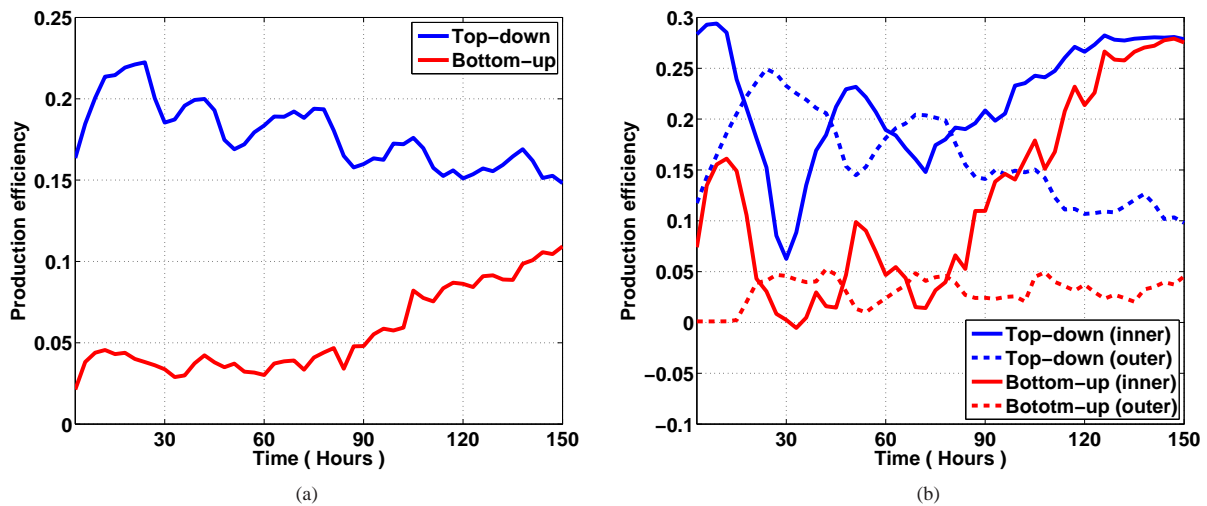


Figure 7. Time series of the area-averaged top-down (blue) and bottom-up (red) APE production efficiency in the surface layer over a) the whole domain; b) the inner region (radius ≤ 1000 km, solid lines) and the outer region (radius > 1000 km, dashed lines).

data from the outer region only is characterised by a gradual decline from 30 hours onward which is more consistent with the time series shown in figure 7a. The gradual reduction of the surface APE production efficiency in the outer region is related to the outward propagating surface outflows described earlier in figure 2. Figure 8 shows the radius-time plot of the top-down APE production efficiency in the lowest model level. The top-down surface APE production efficiency in the outer region dropped from above 0.35 to below 0.05 after each surface outflow event. This suggests the buoyancy of parcels in the outer region was

reduced after the onset of each surface outflow which is consistent to the drop in θ_e shown earlier in figure 2b.

In contrast, the bottom-up sorting method produced a much lower average surface APE production efficiency due to the restriction on the release of surface CAPE during the sorting (figure 7a). The average surface APE production efficiency remained fairly constant at 0.04 in the first 70 hours and then increased gradually to 0.11 by the end of the simulation.

When averaging over the inner region only, the bottom-up surface APE production efficiency showed a rapid increase

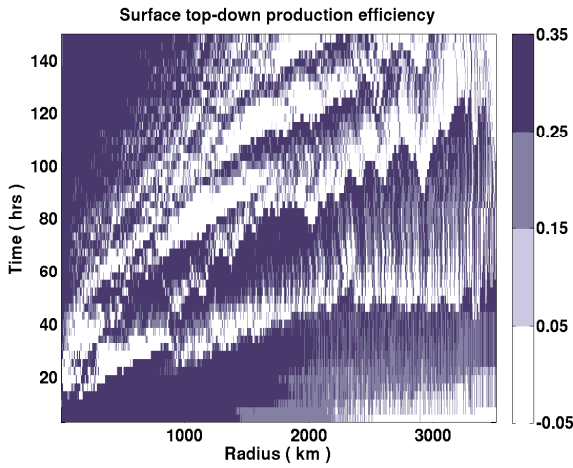


Figure 8. Radius-time plot of top-down production efficiency in the lowest model level.

between 70 and 120 hours and reached similar values to the top-down results by the end of the simulation. This increase was caused by the build up of moisture in the boundary layer of the inner region which lowered the LCL of surface parcels such that they could be saturated by lifting them over a shorter distance. Although the bottom-up sorting method generally restricts the release of CAPE, when constructing the reference state the P_{ref} slots nearer to the surface are usually assigned to the denser surface parcels from the outer region. As a consequence, surface parcels from the inner region can be ‘stacked’ above their original position when using the bottom-up sorting method. Combined with the lowering of LCL, a larger number of surface parcels were able to release CAPE towards the end of the simulation, resulting in a higher average surface APE production efficiency inside the inner region.

When averaging over the outer region only, the bottom-up surface APE production efficiency remained under 0.05 for the entire simulation and showed no clear trend of change. While the top-down results were affected by the outward propagation of surface outflows, the bottom-up results were less sensitive. This is due to the restriction on CAPE release in the bottom-up sorting method such that the reduction in buoyancy associated with the passage of surface outflows will not have a significant impact on the bottom-up results especially in the outer region.

The results above showed that the surface APE production efficiency is controlled predominantly by the sorting method used to produce the reference state. The surface APE production efficiency also showed significant spatial variation between the inner and outer region, with the highest APE production efficiency always located within the inner region. The outward propagation of surface outflows also affected the buoyancy of air parcels in the outer region. However, only the top-down results were sensitive to such process. In the next section, the production of APE by surface fluxes is computed using the surface APE production efficiency.

3.3. Surface APE production

Using the APE production efficiency, the production of APE by surface fluxes is computed following Pauluis (2007). The production of APE by surface sensible and latent heat flux, G_{sen} and G_{lat} respectively, can be computed using

$$G_{sen} = \frac{T_1 - T_{ref}}{T_1} Q_{sen} c_p \rho, \quad (8)$$

$$Q_{sen} = C_T \left(\theta_{surf} - \theta_{\Delta z/2} \right) \left(u^2 + v^2 \right)_{\Delta z/2}^{1/2};$$

$$G_{lat} = \frac{T_1 - T_{ref}}{T_1} Q_{lat} L_v \rho, \quad (9)$$

$$Q_{lat} = C_E \left(r_{v, surf} - r_{v, \Delta z/2} \right) \left(u^2 + v^2 \right)_{\Delta z/2}^{1/2}.$$

In equation (8), Q_{sen} is surface sensible heat flux, c_p is heat capacity and C_T is the dimensionless flux coefficient for sensible heat. In equation (9), Q_{lat} is surface latent heat flux, L_v is latent heat of evaporation and C_E is the dimensionless flux coefficient for moisture. The subscripts $surf$ and $\Delta z/2$ denote that the variable is evaluated at the surface and at a half model level above the surface respectively. Both G_{sen} and G_{lat} have units of Wm^{-2} .

The discussion here will focus on G_{lat} since G_{sen} is relatively insignificant. The radial distribution of surface latent heat flux within the vortex at both 60 and 120 hours is consistent with the typical distribution of wind speed, with the largest values found inside the eyewall and a gradual reduction outwards from the inner region (figure 9a-b). The radial profiles of G_{lat} computed with both sorting methods show a similar distribution with the largest production found in the eyewall. Compared to the surface latent heat flux, the values of G_{lat} are relatively small with roughly 30% of the surface latent heat flux converted into APE. The values of G_{lat} are affected by the difference between the top-down and bottom-up APE production efficiency at the surface which is most obvious at 45 hours. When using the top-down APE production efficiency, positive values of APE production were found just outside the centre of rotation and extended radially outward to as far as 400 km radius. In contrast, little to no APE production was found beyond 50 km radius when using the bottom-up APE production efficiency. This is because the top-down APE production efficiency in the surface layer was generally larger than the bottom-up APE production efficiency especially in the outer region as shown in section 3.2. The difference between the top-down and bottom-up APE production efficiencies in the surface layer became smaller in the inner region as the vortex intensified. At 120 hours, the surface APE productions computed with both efficiencies were almost identical inside the inner region although a slightly larger production was found between 800-1000 km radius with the top-down APE production efficiency.

Figure 10a shows the time series of surface latent heat flux and G_{lat} computed using the top-down and bottom-up production efficiencies. The time series of both the surface latent heat flux and APE productions are computed for the inner region only, which better reflects the vortex’s intensification. The time series of surface latent heat flux showed little change in the first 40 hours, followed by a sharp increase from just above 120 Wm^{-2} to more than 350 Wm^{-2} between 45 and 70 hours as the surface wind speed strengthened during the rapid intensification. Upon reaching a steady state intensity, the surface latent heat flux remained consistently above 350 Wm^{-2} between 70 and 110 before decreasing gradually to below 300 Wm^{-2} towards the end of the simulation. The reduction in surface latent heat flux near the end of the simulation was caused by the decreasing difference in r_v between the boundary layer and the sea surface as well as a slower intensification of the surface wind speed. Both factors reduced the effectiveness of the surface latent heat flux.

Compared to the surface latent heat flux, the values of G_{lat} in the time series were much smaller. While the radial profile (figure 9) showed that as much as 30% of the surface latent heat flux can be converted into APE within the inner region, the time series of both APE productions generally show smaller percentages after including surface parcels with lower production efficiency at larger radii into the calculation when averaging out to 1000 km radius. Figure 10b shows a clearer illustration of both G_{lat} profiles by reducing the range of the y-axis. When using the top-down

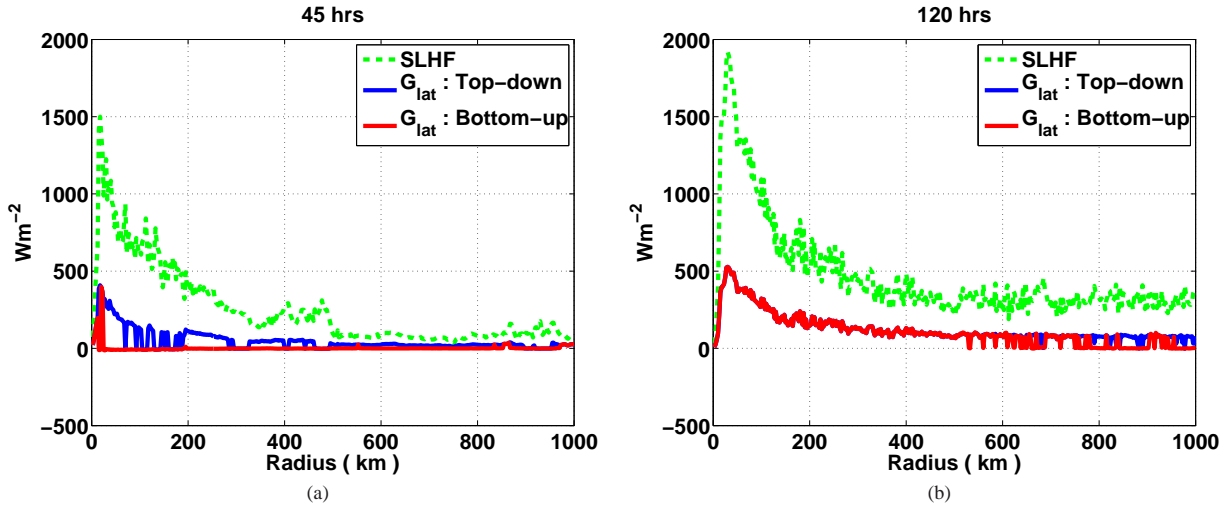


Figure 9. Radial profile of surface latent heat flux (dashed green) and G_{lat} computed using the top-down (solid blue) and bottom-up (solid red) APE production efficiency at a) 45 and b) 120 hours. Note that the profiles extend to 1000 km radius only for clarity.

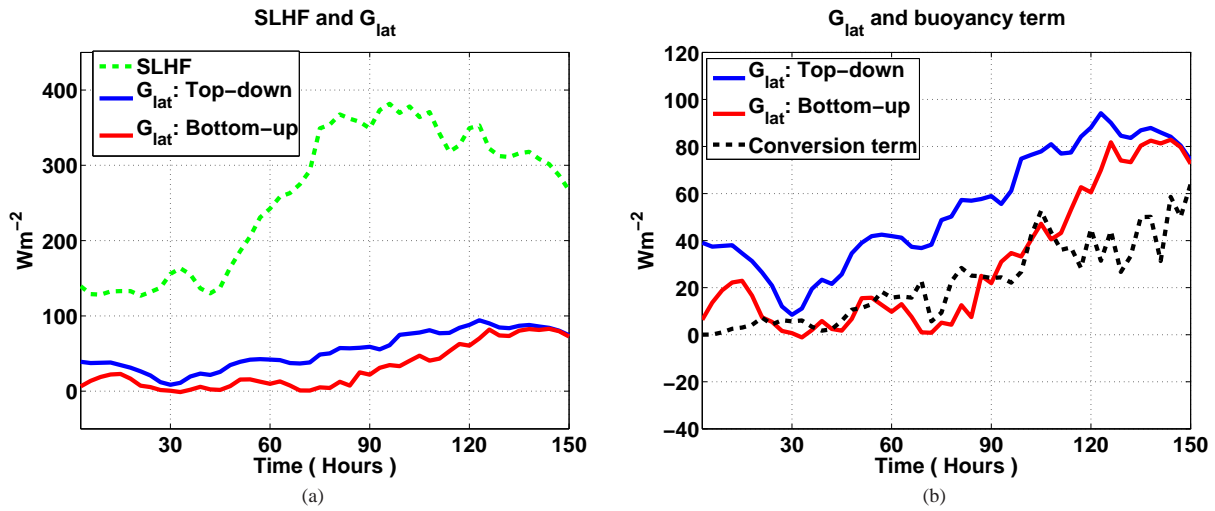


Figure 10. Time series of a) surface latent heat flux (SLHF, dashed green) and G_{lat} computed using the top-down (solid blue) and bottom-up (solid red) APE production efficiency; b) Time series of G_{lat} as in (a) and the conversion term $C_{APE \rightarrow KE}$ (dashed black).

APE production efficiency, the G_{lat} profile was generally larger than that computed with the bottom-up APE production efficiency which is consistent with the radial profile shown previously in figure 9. The top-down G_{lat} profile showed a marked increase between 40–60 hours as the vortex rapidly intensified. This was followed by a steady increase until 120 hours and a slight decline near the end of the simulation.

Since the top-down surface APE production efficiency was affected by the outward propagating surface outflows, the values of top-down G_{lat} also showed similar variation. Figure 11 shows the radius-time plot of the values of G_{lat} computed with the top-down APE production efficiency. Similar to the radial profile shown previously in figure 9a–b, the inner region within 1000 km radius was dominated by relatively large values of G_{lat} while little to no G_{lat} was found beyond 2500 km radius. The region between 1000 and 2500 km radius was characterised by alternating bands of higher (greater than 10 Wm^{-2}) and lower (less than 10 Wm^{-2}) G_{lat} values. The transition from higher to lower values of G_{lat} is quite rapid due to the rapid drop in the top-down APE production efficiency after the onset of surface outflow associated with each passing surface outflow.

Compared to the top-down APE production time series, the bottom-up APE production time series mostly has smaller values, especially during the first 100 hours of simulation. Also, the bottom-up APE production showed only a modest increase during the rapid intensification period between 40–60 hours compared

to the top-down APE production time series. The rise in bottom-up APE production began later at 70 hours and showed a steady increase until 120 hours, followed by a slight decline near the end of the simulation similar to the top-down APE production. The delayed rise of bottom-up APE production is consistent with the time series of the bottom-up APE production efficiency (figure 7) which showed a much lower APE production efficiency in the first 70 hours of the simulation followed by a gradual increase afterwards.

Finally, the production of APE by surface latent heat flux is compared to the conversion into kinetic energy ($C_{APE \rightarrow KE}$). The conversion term $C_{APE \rightarrow KE}$ is defined using the term representing buoyancy force in the vertical momentum equation :

$$C_{APE \rightarrow KE} = \rho g w \left(\frac{\theta - \bar{\theta}}{\bar{\theta}} + 0.61(q_v - \bar{q}_v) - q_l - \frac{c_p \bar{\theta}_v}{g} \frac{\partial \pi_r}{\partial z} \right). \quad (10)$$

In brief, the first and second terms on the RHS of equation (10) represent the contribution to buoyancy force from the deviation of θ and q_v from the initial state $\bar{\theta}$ and \bar{q}_v while the third term represents the work required to carry the liquid water loading. The last term is a ‘correction’ term needed to obtain the true buoyancy at a given integration time since the model domain will become warmer and more humid relative to the initial state as the vortex develops. This correction is made using the vertical gradient of

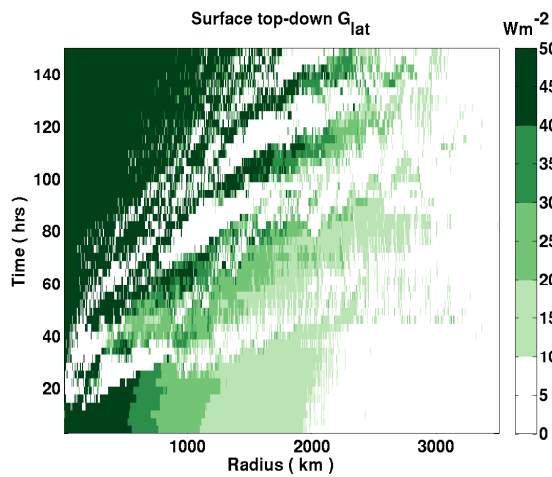


Figure 11. Radius-time plot of top-down G_{lat} in the lowest model level.

the Exner pressure deviation term $\partial\pi_r/\partial z$ which is positive for an atmosphere that is warmer than the initial state thus lowering the buoyancy term and vice versa. A more detailed discussion on the role of buoyancy force and the correction term in the vertical kinetic energy budget is provided in the appendix.

The time series of the conversion term, integrated over the volume of the inner region, is provided in figure 10b. In general, the conversion term increased gradually as the vortex intensified. Compared to the APE production time series, the bottom-up time series clearly shows a closer match to the conversion term, especially during the first 100 hours of the simulation. This suggests that when using the bottom-up sorting method, the APE budget was dominated by the balance between APE production and the conversion term while the $dAPE/dt$ term was relatively small. However, the bottom-up G_{lat} became greater than the conversion term in the last 30 hours of the simulation. This was caused by the gradual increase in the bottom-up surface APE production efficiency especially in the inner region as shown previously in figure 7.

In contrast, the top-down APE production is always larger than the conversion term throughout the entire simulation, indicating a build up of APE in the domain. Therefore, the $dAPE/dt$ will be more significant in the APE budget due to the larger APE production resulting from the top-down sorting method.

The results above suggest the bottom-up sorting method is more capable in identifying the portion of APE generated by surface latent heat flux that can be converted into kinetic energy through the work of buoyancy force. The top-down sorting method, in contrast, tends to produce a much larger surface APE production as it assumes all surface CAPE in the vortex can be released, resulting a larger production efficiency at the surface. However, a large portion of surface CAPE is dynamically inert, especially in regions dominated by subsidence further away from the centre of rotation. The large APE production in the top-down sorting method can only contribute to the storage term instead of converting into kinetic energy. Therefore, the conclusion here is that the bottom-up sorting method is a more suitable way to construct the reference state as it is able to minimise $dAPE/dt$.

4. Conclusion and discussion

How to construct the reference state in moist APE theory has been a longstanding vexing issue. We investigated this here in connection with the energetics of TC intensification and MPI theory. Until now, the prevailing view had been that the reference state should be constructed as the one minimising potential energy in an adiabatic re-arrangement of the fluid parcels, in accordance with Lorenz (1955)'s original recommendation. Although various

authors such as Lorenz (1978), Randall and Wang (1992) and Tailleux and Grandpeix (2004) have discussed various ways to construct such a reference state, the implications for our understanding of moist energetics have been limited so far to rather abstract considerations about how to generalise the concept of CAPE in a one-dimensional atmosphere for which all the APE resides in its vertical component. Discussions of the implications of the choice of any particular reference state for our understanding of the energetics of concrete weather phenomena have been lacking.

In this study, two different sorting strategies were used to construct the reference state, referred to as the bottom-up and top-down sorting approaches, similarly to what was recently done for an ocean with a nonlinear equation of state by Saenz *et al.* (2015). In contrast to the oceanic case for which the two different approaches yield similar reference states, large differences exist between the bottom-up and top-down reference states in our simulation of TC intensification. This difference has important consequences for our understanding of the thermodynamic efficiency associated with the different diabatic processes at work in a TC and for trying to predict how much APE can contribute to the intensification.

As can be expected, the top-down reference state is the one that leads to the largest value of APE, since it is by construction the one that can incorporate most if not all the CAPE present in the domain, and therefore the one that the prevailing wisdom would recommend to use in moist APE theory. However, it is important to recognise that CAPE contributes to moist energetics only when parcels are able to reach their level of free convection, and hence when they have become absolutely unstable. The main problem with the top-down based definition of APE is that it incorporates a large fraction of the total CAPE that is in fact dynamically inert and not actually available for conversion into kinetic energy. Many such parcels can be found in the regions of the TC dominated by subsidence, where CAPE is difficult if not impossible to release. In contrast, the bottom-up based definition of APE only includes the CAPE of the absolutely unstable parcels, when such parcels have actually started to rise in updraughts. As a result, the top-down sorting method tends to overestimate the thermodynamic efficiency of the system, and hence to lead to an APE generation term that is much larger than the actual conversion of APE into kinetic energy. A much better agreement between APE generation and subsequent conversion into kinetic energy is found when using the bottom-up sorting method. Therefore, while the use of the top-down reference state might be preferable as a way to synthesise information about all available potential energy contained in the system, it nevertheless yields a less satisfactory description of the energetics of TC intensification for which it appears preferable to include as part of the APE definition only part of the APE actually convertible into kinetic energy.

The present results have two important implications. First, they establish that the common approach of defining the reference state as one that minimises the potential energy in an adiabatic re-arrangement may not be the most suitable approach, and that it is much better in the present example to define it such as to minimise $dAPE/dt$ in order to maximise the correlation between APE generation and conversion of APE into kinetic energy; our results suggest that the bottom-up sorting approach allows one to achieve this objective. Second, they imply that we can provide a more rigorous footing for the MPI theory using APE theory; this will be investigated in future studies.

Appendix

A. Buoyancy force and the vertical kinetic energy budget

The key result presented in this paper is that given a suitable reference state, the production of APE by surface latent heat flux is mostly balanced by the conversion into kinetic energy through the work of buoyancy force. Such conversion takes place via the vertical momentum equation, which in the 2D model is given by

$$\frac{Dw}{Dt} = g \left(\frac{\theta - \bar{\theta}}{\bar{\theta}} + 0.61(q_v - \bar{q}_v) - q_l \right) - c_p \bar{\theta}_v \frac{\partial \pi}{\partial z} + D_w, \quad (11)$$

where w is vertical velocity, g is gravity, $\bar{\theta}$ and \bar{q}_v are the initial potential temperature and vapour mixing ratio profiles used to initialise the model domain, q_l is liquid water mixing ratio, c_p is heat capacity, $\bar{\theta}_v$ is the initial virtual potential profile, π is the Exner pressure deviation from the initial pressure profile and D_w is **diffusion of vertical kinetic energy**. Using the vertical momentum equation, the vertical kinetic energy budget can be defined as

$$\begin{aligned} \frac{DKE_w}{Dt} = w m g \left(\frac{\theta - \bar{\theta}}{\bar{\theta}} + 0.61(q_v - \bar{q}_v) - q_l \right) \\ - m w c_p \bar{\theta}_v \frac{\partial \pi}{\partial z} + w m D_w, \end{aligned} \quad (12)$$

where $KE_w = 0.5mw^2$ is the vertical kinetic energy and m is mass. Equation (12) shows that the vertical kinetic energy budget is controlled by three terms on the right hand side that **represent the work of buoyancy force, the work of vertical PGF and diffusion of vertical kinetic energy** respectively. Note that the **work of buoyancy force** in equation (12) is defined using the deviation of θ and q_v from the initial profiles $\bar{\theta}$ and \bar{q}_v . Both deviation terms are generally positive due to the continuous heating and moistening of the model domain as the vortex intensified. Therefore, the **work of buoyancy force** is a source of KE_w for an ascending air parcel with positive w . Meanwhile, $\partial \pi / \partial z$ is usually positive due to the less rapid drop of air pressure in the mid-atmosphere compared to the surface. Therefore, the **work of vertical PGF and the diffusion of vertical kinetic energy** are net sinks of KE_w for an ascending air parcel.

Since the **work of buoyancy force** is clearly a source of KE_w , it is therefore a suitable representation of the portion of APE that is converted into vertical kinetic energy (i.e. the conversion term $C_{APE \rightarrow KE}$). However, a key problem here is that the **work of buoyancy force in equation (12) is defined with respect to the $\bar{\theta}$ and \bar{q}_v profiles which are time independent while the reference state and associated APE production efficiency evolve with time. In order to link the conversion term to the time dependent reference state and the APE production term, the work of buoyancy force in equation (12) is redefined with respect to a time-dependent horizontally-averaged Exner pressure field. The Exner pressure deviation (π) is divided into a time-dependent horizontal average across the vortex (π_r) and a local deviation (π') such that $\pi = \pi_r + \pi'$. The vertical kinetic energy budget can then be written as**

$$\begin{aligned} \frac{DKE_w}{Dt} = w m g \left(\frac{\theta - \bar{\theta}}{\bar{\theta}} + 0.61(q_v - \bar{q}_v) - q_l - \frac{c_p \bar{\theta}_v}{g} \frac{\partial \pi_r}{\partial z} \right) \\ - m w c_p \bar{\theta}_v \frac{\partial \pi'}{\partial z} + w m D_w. \end{aligned} \quad (13)$$

The $\partial \pi_r / \partial z$ term in the first term on the RHS of equation (13) acts as a correction that removes the extra buoyancy with respect

to the time independent initial profiles. **By incorporating it into the term representing the work of buoyancy force (i.e. first term on the RHS of equation (13)), it can then be used for a fair comparison with the time dependent APE production term as in equation (10).**

References

- Bryan GH, Rotunno R. 2009. The maximum intensity of tropical cyclones in axisymmetric numerical model simulations. *Mon. Wea. Rev.* **137**: 1770–1789.
- Craig GC. 1996. Numerical experiments on radiation and tropical cyclones. *Q.J.R. Meteorol. Soc.* **112**: 415–422.
- Craig GC, Gray SL. 1996. CISK or WISHE as a mechanism for tropical cyclone intensification. *J. Atmos. Sci.* **53**: 3528–3540.
- Emanuel KA. 1986. An air-sea interaction theory for tropical cyclones. part I: Steady-state maintenance. *J. Atmos. Sci.* **43**: 585–605.
- Emanuel KA. 1988. The maximum intensity of hurricanes. *J. Atmos. Sci.* **45**(7): 1143–1155.
- Emanuel KA. 1991. The theory of hurricanes. *Annu. Rev. Fluid Mech.* **23**: 179–196.
- Emanuel KA. 1994. *Atmospheric convection*. Oxford Univ. Press: New York.
- Emanuel KA. 2003. Tropical cyclones. *Annu. Rev. Earth Planet Sci.* **31**: 75–104.
- Jordan CL. 1958. Mean soundings for the West Indies area. *J. Meteor.* **15**: 91–97.
- Lorenz EN. 1955. Available potential energy and the maintenance of the general circulation. *Tellus* **7**: 157–167.
- Lorenz EN. 1978. Available potential energy and the maintenance of a moist circulation. *Tellus* **30**: 15–31.
- Lorenz EN. 1979. Numerical evaluation of moist available energy. *Tellus* **31**: 230–235.
- Nguyen VS, Smith RK, Montgomery MT. 2008. Tropical-cyclone intensification and predictability in three dimensions. *Q.J.R. Meteorol. Soc.* **134**: 563–582.
- Ozawa H, Ohmura A, Lorenz R, Pujol T. 2003. The second law of thermodynamics and the global climate system: a review of the maximum entropy production principle. *Rev. Geophys.* **41**: 1018–1024.
- Ozawa H, Shimokawa S. 2015. Thermodynamics of a tropical cyclone: generation and dissipation of mechanical energy in a self-driven convection system. *Tellus A* **67**: 24216.
- Pauluis O. 2007. Sources and sinks of available potential energy in a moist atmosphere. *J. Atmos. Sci.* **135**: 1697–1714.
- Peng J, Zhang L, Zhang Y. 2015. On the local available energetics in a moist compressible atmosphere. *J. Atm. Sci.* **72**: 1551–1561.
- Randall DA, Wang JY. 1992. The moist available energy of a conditionally unstable atmosphere. *J. Atmos. Sci.* **49**: 240–255.
- Rotunno R, Emanuel KA. 1987. An air-sea interaction theory for tropical cyclones. part II: Evolutionary study using a nonhydrostatic axisymmetric numerical model. *J. Atmos. Sci.* **4**: 542–561.
- Saenz JA, Tailleux R, Butler ED, Hughes GO, Oliver KIC. 2015. Estimating Lorenz's reference state in an ocean with a nonlinear equation of state for seawater. *J. Phys. Oceanogr.* **45**: in press.
- Shin SL, Smith RK. 2008. Tropical cyclone intensification and predictability in a minimal three dimensional model. *Q.J.R. Meteorol. Soc.* **134**: 1661–1671.
- Smith RK, Montgomery MT, Vogl S. 2008. A critique of Emanuel's hurricane model and potential intensity theory. *Q.J.R. Meteorol. Soc.* **134**: 551–561.

- Tailleux R. 2010. Entropy versus APE production: on the buoyancy power input in the ocean energy cycle. *Geophys. Res. Lett.* **37**: L22 603.
- Tailleux R. 2013a. Available potential energy and exergy in stratified fluids. *Ann. Rev. Fluid Mech.* **45**: 35–58.
- Tailleux R. 2013b. Available potential energy density for a multicomponent Boussinesq fluid with arbitrary nonlinear equation of state. *J. Fluid Mech.* **735**: 1832–1852.
- Tailleux R, Grandpeix J. 2004. On the seemingly incompatible parcel and globally integrated views of the energetics of triggered atmospheric deep convection over land. *Q.J.R. Meteorol. Soc.* **130**: 3223–3243.